Supplementary Information: Long-distance atmospheric transport of microplastic fibres depends on their shapes

Shuolin Xiao[1], Yuanfeng Cui[1], Janice Brahney[2], Natalie M. Mahowald[3] and Qi Li[1*]

[1*]School of Civil and Environmental Engineering, Cornell University, 527 College Avenue, Ithaca, 14853, NY, USA.
[2]Department of Watershed Sciences, Utah State University, 5200 Old Main Hill, Logan, 84322, UT, USA.
[3]Department of Earth and Atmospheric Sciences, Cornell University, 112 Hollister Drive, Ithaca, 14853, NY, USA.

*Corresponding author(s). E-mail(s): ql56@cornell.edu;

Supplementary Note 1: Settling velocity and mobility matrix of MPFs

In the spherical coordinate system, through the azimuthal angle θ and polar angle ϕ of one single MPF defined in the main text, equation **??** can be reorganized in a component-wise form as:

$$w_{f,1} = (M_{\parallel} - M_{\perp}) \cos\phi \sin\theta 2lA_f(\rho_f - \rho_a)g \tag{1}$$

$$w_{f,2} = (M_{\parallel} - M_{\perp}) \sin\phi \sin\theta 2lA_f(\rho_f - \rho_a)g \tag{2}$$

$$w_{f,3} = [M_{\perp} + (M_{\parallel} - M_{\perp}) \cos^2\theta] 2lA_f(\rho_f - \rho_a)g \tag{3}$$

The mobility coefficients of MPFs have a general expression for all the microplastics fibers including the one with finite Re_l has the formulation as shown below [1–3]:

$$M_{\parallel} = \frac{ln\beta}{4\pi\mu l}[1 - \frac{F_{\parallel}}{ln\beta} + O(\frac{1}{ln^2\beta})] \tag{4}$$

$$M_{\perp} = \frac{ln\beta}{8\pi\mu l}[1 - \frac{F_{\perp}}{ln\beta} + O(\frac{1}{ln^2\beta})] \tag{5}$$

where μ is the dynamic viscosity of air and

$$F_{\parallel} = \frac{1}{2}\Big[\frac{E_1(2Re_l) + ln(2Re_l) - e^{-2Re_l} + \gamma + 1}{2Re_l} + E_1(2Re_l) + ln(Re_l) + \gamma - 3ln2 + 1 + 6ln\frac{\pi(b+c)}{4\int_0^b \sqrt{1 + \frac{c^2x^2}{b^2(b^2-x^2)}}dx} + 2\frac{b-c}{b+c}] \tag{6}$$

$$F_{\perp} = E_1(Re_l) + ln(Re_l) - \frac{e^{-Re_l} - 1}{Re_l} + \gamma - \frac{1}{2} - ln4 + ln\frac{\pi(b+c)}{4\int_0^b \sqrt{1 + \frac{c^2x^2}{b^2(b^2-x^2)}}dx} + \frac{1}{2}\frac{b-c}{b+c} \tag{7}$$

Note that the last term in equation 6 accounts for the elliptical cross section of the microplastic fiber, which vanishes when the microplastic fiber is in a round configuration at the cross section. Here γ is Euler's constant and E_1 is the exponential integral function

$$E_1(x) = \int_x^{\infty} \frac{e^{-t}}{t}dt \tag{8}$$

The derivation of the last term in equation 6 for flat fiber follows the works of [2] and [3]. The local cross-sectional shape correction for flat fiber are the terms in equation 6.4 of [3] listed below:

$$2\mathbf{e} \cdot \int_{-1}^{1} \mathbf{K}(s)ds + cos\theta\mathbf{p}\int_{-1}^{1} lnK(s)ds \tag{9}$$

Here $\mathbf{e}$ is the unit directional vector of the slip velocity between microplastic fiber and ambient flow, denoted as (0, 0, 1). The s is the dimensionless distance along the fiber centerline. $\mathbf{K}(s)$ and $K(s)$ are the cross-sectional shape factors given by [2] in equations 5.6 and 6.8 as $lnK = \pi(b+c)/4\int_0^b \sqrt{1 + \frac{c^2x^2}{b^2(b^2-x^2)}}dx$ and $K_{ij} = \delta_{ij}(\pi(b+c)/4\int_0^b \sqrt{1 + \frac{c^2x^2}{b^2(b^2-x^2)}}dx + \frac{1}{2}(b-c)/(b+c) - \Gamma_i\Gamma_j\frac{1}{2}(b-c)/(b+c)$, respectively. $\mathbf{\Gamma}$ is the unit directional vector of the larger principal diameter of the ellipse (2b), which we assume to be in horizontal direction to make the projected area and hence the drag force contributed by the cross section of the microlastic fiber along the settling direction always the largest and in a stable equilibrium position. Since the microplastic fiber we considered are assumed to have a uniform distribution along the fiber length. The above equation can be simplified as

$$4\mathbf{e} \cdot \mathbf{K} + 2cos\theta\mathbf{p}lnK \tag{10}$$

With mathematical manipulation, the equation 10 can be formulated explicitly as:

$$4ln\frac{\pi(b+c)}{4\int_0^b\sqrt{1+\frac{c^2x^2}{b^2(b^2-x^2)}}dx}+2\frac{b-c}{b+c}+2\cos^2\theta ln\frac{\pi(b+c)}{4\int_0^b\sqrt{1+\frac{c^2x^2}{b^2(b^2-x^2)}}dx} \tag{11}$$

The expressions of mobility coefficients have simplified form in the limit of creeping flow regime and low Reynolds number Re_l regime [1, 3].

In the limit of creeping flow

$$M_{\parallel}=\frac{ln\beta}{4\pi\mu l}[1+(ln4-1.5-3ln\frac{\pi(b+c)}{4\int_0^b\sqrt{1+\frac{c^2x^2}{b^2(b^2-x^2)}}dx}-\frac{b-c}{b+c})/ln\beta+O(\frac{1}{ln^2\beta})] \tag{12}$$

$$M_{\perp}=\frac{ln\beta}{8\pi\mu l}[1+(ln4-0.5-ln\frac{\pi(b+c)}{4\int_0^b\sqrt{1+\frac{c^2x^2}{b^2(b^2-x^2)}}dx}-\frac{1}{2}\frac{b-c}{b+c})/ln\beta+O(\frac{1}{ln^2\beta})] \tag{13}$$

In the limit of low Reynolds number Re_l

$$M_{\parallel}=\frac{ln\beta}{4\pi\mu l}[1+(ln4-1.5-Re_l/4-3ln\frac{\pi(b+c)}{4\int_0^b\sqrt{1+\frac{c^2x^2}{b^2(b^2-x^2)}}dx}-\frac{b-c}{b+c})/ln\beta+O(\frac{1}{ln^2\beta},\frac{Re_l^2}{ln\beta})] \tag{14}$$

$$M_{\perp}=\frac{ln\beta}{8\pi\mu l}[1+(ln4-0.5-Re_l/2-ln\frac{\pi(b+c)}{4\int_0^b\sqrt{1+\frac{c^2x^2}{b^2(b^2-x^2)}}dx}-\frac{1}{2}\frac{b-c}{b+c})/ln\beta+O(\frac{1}{ln^2\beta},\frac{Re_l^2}{ln\beta})] \tag{15}$$

Supplementary Note 2: Simplification of the settling velocity formulation for climate model implementation

Furthermore, if we ignore the turbulence effect and define $K_c = ln\frac{\pi(b+c)}{4\int_0^b\sqrt{1+\frac{c^2x^2}{b^2(b^2-x^2)}}dx}-\frac{1}{2}\frac{b-c}{b+c}$ that has zero value for round fiber, the resulting settling velocity w_s of MPF can be simplified as following,

$$w_s=\frac{ln\beta}{4\pi\mu}A_f(\rho_f-\rho_a)g*\begin{cases}(1+\frac{ln4-0.5-Re_l/2-K_c}{ln\beta}) & \text{for } Re_l<1\\ (1-\frac{E_1(Re_l)+ln(Re_l)-\frac{e^{-Re_l}-1}{Re_l}+\gamma-\frac{1}{2}-ln4-K_c}{ln\beta}) & \text{for } 1\le Re_l\le 4\\ (1-\frac{ln(Re_l)+1/Re_l+\gamma-0.5-ln4-K_c}{ln\beta}) & \text{for } Re_l>4\end{cases} \tag{16}$$

Here E_1 is the exponential integral function and it is defined as $E_1(x) = \int_x^\infty\frac{e^{-t}}{t}dt$. As a consequence, for the micro-plastic fiber settling in air, when inertial effect is significantly dominate over turbulence effect, the micro-plastic fiber will prefer to settle with its long axis parallel to the horizontal plane, leading to the magnitude of the settling velocity of micro-plastic fiber approximate to the formulation given by equation 16, which can be directly utilized in climate model for its simplicity.

Supplementary Note 3: Characteristic time scale of MPF

The typical timescale for rotations of small MPFs due to turbulence τ_{turb} is the Kolmogorov timescale

$$\tau_{turb} = (\frac{\nu}{\epsilon})^{1/2} \tag{17}$$

Where ϵ is the local turbulent dissipation rate.

For $\tau_{sed,\theta=45^\circ}$ of MPF with low Reynolds number Re_l, it can be expressed as [4, 5]:

$$\tau_{sed,45^\circ} = \frac{8\nu ln2\beta}{5w_{f,min}^2} \tag{18}$$

Here $w_{f,min}$ corresponds the settling velocity magnitude when MPF settles with $\theta = 90^\circ$.

With equation 17 and equation 18, we can get the explicit expression of S_F as

$$S_F = \frac{5w_{f,min}^2}{8\nu ln2\beta}(\frac{\nu}{\epsilon})^{1/2} \tag{19}$$

For MPF with long-axis length scale larger than the Kolmogorov length scale, the appropriate turbulence time scale τ_{turb} can be derived as following [6]:

(a)at the inertial range, the time scale of turbulence over fiber with long-axis length L is $(\frac{L^2}{\epsilon})^{1/3}$.

(b)at the dissipation range, the time scale of turbulence over MPF with long-axis length L is

$$\tau_\eta = (\frac{\eta^2}{\epsilon})^{1/3} = (\frac{L^2}{\epsilon})^{1/3} \tag{20}$$

The Kolmogrov length scale η is replaced by the fiber long-axis length L if they are the same. Therefore, we can expect, for fiber size on the scale of Kolmogorov length scale (the regime between dissipation range and inertial range),the related time scale is $(\frac{L^2}{\epsilon})^{1/3}$.

The finite Re_l correction of the fiber settling time scale $\tau_{sed,\theta=45^\circ}$ can be derived as following based on the idea from [4, 5]. When MPF settles in turbulence, it experiences three toques including the inertial torque, rotational drag torque, and a torque from turbulent strain [4, 5]. For MPF with finite Reynolds number Re_l, the corresponding zero-torque tumbling rate determined by inertial torque and rotational drag torque can be expressed as [1, 3]:

$$\dot{\mathbf{p}}_{inertial} = F_{ic}(Re_l;\ \alpha)\frac{5Re_l(\hat{\mathbf{e}_w} \cdot \mathbf{p})}{8lln(\beta)}\mathbf{w}_f \cdot (\mathbf{I} - \mathbf{pp}) \tag{21}$$

with

$$F_{ic}(Re_l;\ \alpha) = -\frac{12}{5Re_l^2}\left(\frac{1}{2(1-c_\alpha)}\left\{2+2\frac{e^{-Re_l(1-c_\alpha)}-1}{Re_l(1-c_\alpha)} - E_1[Re_l(1-c_\alpha)] - ln[Re_l(1-c_\alpha)] - e\right\} + \frac{1}{2(1+c_\alpha)}\left\{2+2\frac{e^{-Re_l(1+c_\alpha)}-1}{Re_l(1+c_\alpha)} - E_1[Re_l(1+c_\alpha)] - ln[Re_l(1+c_\alpha)] - e\right\} - \frac{1}{(1-c_\alpha)c_\alpha}\left[1-\frac{1-e^{-Re_l(1-c_\alpha)}}{Re_l(1-c_\alpha)}\right] + \frac{1}{(1+c_\alpha)c_\alpha}\left[1-\frac{1-e^{-Re_l(1+c_\alpha)}}{Re_l(1+c_\alpha)}\right]\right) \tag{22}$$

Note that equation 22 has identical expression for round fiber and flat fiber[2, 3], which can be demonstrated via lnK and $\mathbf{K}$ introduced previously. Here α is the angle between $\mathbf{p}$ and $\mathbf{w}_f$ and $c_\alpha = cos\alpha$. As defined by [4, 5], the typical time scale of rotations due to sedimentation can be given as the inverse of this tumbling rate:

$$\tau_{sed,45^\circ} = \frac{8\nu ln\beta}{5F_{ic}(Re_l;\ 45^\circ)w_{f,min}^2} \tag{23}$$

In conclusion, the formulation of S_F can be expressed for both low Reynolds number Re_l and finite Reynolds number Re_l as follows:

$$S_F = \begin{cases} \frac{5w_{f,min}^2}{8\nu ln2\beta}(\frac{\nu}{\epsilon})^{1/2} & \text{low Reynolds number } Re_l \\ \frac{5F_{ic}(Re_l;\ 45^\circ)w_{f,min}^2}{8\nu ln\beta}(\frac{L^2}{\epsilon})^{1/3} & \text{finite Reynolds number } Re_l \end{cases} \tag{24}$$

The dominance of inverse of Kolmogorov time scale over mean velocity gradient $\mathbf{S}$ can be demonstrated as follows: in the extreme case

$$\mid \mathbf{S} \mid = (\epsilon/\nu)^{1/2} \tag{25}$$

For the typical dissipation rate within the atmospheric boundary layer (not too close to the wall) $\epsilon \sim 10^{-3}m^2/s^3$, which requires the variation of velocity magnitude as $10m/s$ within a one-meter scale. This is not the case that occurred within the atmospheric boundary layer. Also, as shown by [7], the ratio of $\nu \mid \mathbf{S} \mid^2 /\langle\epsilon\rangle$ decrease as a function of Reynolds number of the atmospheric boundary layer. The typical ratio is less than 0.1. This confirms the dominance of turbulence over mean velocity gradient (or relies on velocity profile within the surface layer).

Supplementary Note 4: Discussion on source attribution

It is interesting that the flat case represents a more extreme shift than seen in the small case previously, which seems counterintuitive: one would expect the largest difference in sources between the largest and smallest sizes. This appears to be because of a non-linearity in the combination of the transport model and optimal estimation as a function of size. Sensitivity tests using only plastics in one bin at a time show that the optimal estimation predicts the largest contribution from the ocean source when the plastic particles are primarily 17.5 μm in equivalent diameter (Fig. 1). This is because of the combination of two offsetting processes: smaller plastics can travel farther from the far-away ocean sources, so more ocean-derived plastics can contribute at the sites as plastics are modeled at a smaller size. But if plastics are all small, then all sources can travel farther, and there is less source needed to obtain the same deposition at remote sites.

Supplementary Figure 1

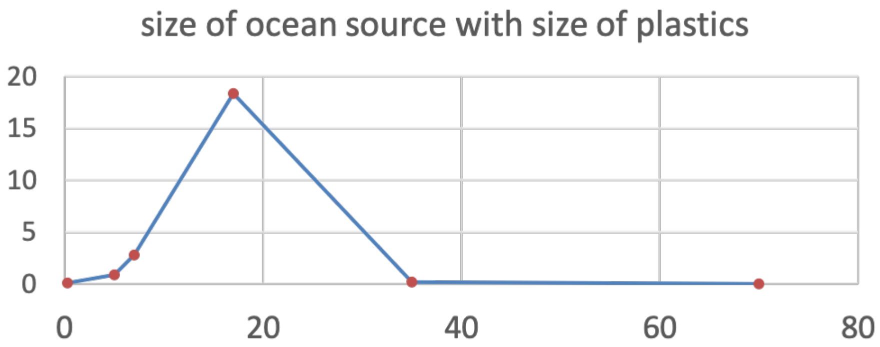

Fig. 1 Figure showing the size of the ocean source (Tg on the y axis) as a function of the size of plastics (um on x-axis) in sensitivity studies where all plastics are assumed to be one size for each sensitivity study.

Supplementary Figure 2

References

[1] Lopez, D., Guazzelli, E.: Inertial effects on fibers settling in a vortical flow. Physical Review Fluids **2**(2), 024306 (2017)

[2] Batchelor, G.: Slender-body theory for particles of arbitrary cross-section in stokes flow. Journal of Fluid Mechanics **44**(3), 419–440 (1970)

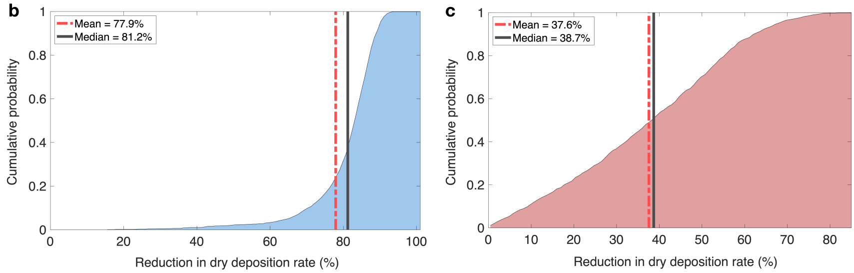

Fig. 2 Cumulative probability distributions of (a) the reduction in dry deposition rate for MPF with a flat bottom and (b) the reduction in dry deposition rate for MPF with round cross-section. Note that the reduction in a dry deposition for MPF with a flat bottom is evaluated between w_s calculated from our model for MPF with a flat bottom and the one obtained from our model but with a presumption that the cross-section is in a round shape based on the sampled fiber on site. The reduction in dry deposition for MPF with a round cross-section is compared between w_s calculated from our model and the one obtained from the volumetric spherical particle model. For all the subfigures, red dash-dot lines denote the mean quantities and black solid lines represent the median values.

[3] Khayat, R., Cox, R.: Inertia effects on the motion of long slender bodies. Journal of Fluid Mechanics **209**, 435–462 (1989)

[4] Kramel, S.: Non-spherical particle dynamics in turbulence (2018)

[5] Menon, U.K.: Theory and simulation for the orientation of high aspect ratio particles settling in homogeneous isotropic turbulence. PhD thesis, Cornell University (2009)

[6] Tennekes, H., Lumley, J.: A First Course in Turbulence, (1972). https://doi.org/10.7551/mitpress/3014.001.0001

[7] Hebert, D.A., de Bruyn Kops, S.M.: Relationship between vertical shear rate and kinetic energy dissipation rate in stably stratified flows. Geophysical research letters **33**(6) (2006)